Coadsorption phase diagram for Kr/CCl_4 on graphite

William J. Weber* and David L. Goodstein
Condensed Matter Physics 114-36, California Institute of Technology, Pasadena, California 91125
(Received 29 September 2001; revised manuscript received 10 June 2002; published 25 October 2002)

We present the results of an extensive calorimetric study of krypton coadsorbed on graphite precoated with a saturated monolayer of carbon tetrachloride. Combining the heat capacity data with film equation of state measurements from a previous study [W. J. Weber and D. L. Goodstein, Phys. Rev. Lett. **83**, 3888 (1999)] permits construction of the Kr/CCl_4 coadsorption phase diagram between 77 and 130 K. Kr succeeds in displacing the CCl_4 from the surface, by a continuous process which results, at lower temperatures, in a film indistinguishable from that of pure Kr adsorbed on graphite. At higher temperatures, a new first-order phase transition, unique to the coadsorption system, is observed and likely indicates a transition to a mixed Kr/CCl_4 film. Finally, measurements at higher Kr coverages reveal evidence for a high temperature extension of the reentrant layering phenomena previously observed for Kr on graphite.

DOI: 10.1103/PhysRevB.66.165419 PACS number(s): 68.43.−h, 68.35.Rh, 64.75.+g, 64.30.+t

I. INTRODUCTION

Coadsorption of Kr and CCl_4 on graphite is one of a number of two component films exhibiting an interesting phenomenon known as displacement.[1,2] In such systems, a preadsorbed monolayer of a strongly adsorbing material, such as CCl_4, SF_6, or C_6H_{12}, is observed to be displaced from a graphite substrate by a relatively inert gas, such as Kr, Xe, or CH_4.[3–9] Displacement's signature in volumetric coadsorption isotherms, which measure the film coverage of the inert gas species as a function of its vapor pressure or chemical potential, consists of a suppression of the inert gas adsorption at low chemical potentials followed by a ''reaquisition'' of the pure inert gas isotherm at higher pressures. For Kr/CCl_4 at 80 K, for instance, there is little Kr adsorption observed at the pressure of pure Kr monolayer condensation on bare graphite.[1] At nearly 500 times this pressure, however, a first-order condensation of Kr is observed, followed by second and higher layer condensations occurring at the same pressures as observed for Kr on bare graphite. This recovery of the pure Kr adsorption behavior implies that Kr succeeds in adsorbing on bare graphite at the expense of the much more strongly adsorbed CCl_4, which has been displaced.

The nonwetting nature of the preadsorbate, CCl_4 in this case, simplifies the coadsorption thermodynamics and provides the mechanism behind displacement. CCl_4 wets graphite only partially at low temperature, saturating and forming bulk crystals in coexistence with a film of only monolayer thickness.[10,11] A full monolayer of such an adsorbate thus coexists with its own bulk crystals, allowing transfer of molecules between monolayer film and bulk solid phases with no cost in free energy. Thus the total system free energy may be lowered if molecules from the preadsorbate monolayer are displaced into the bulk phase and thereby allow the weakly attracted inert species to adsorb directly onto the bare substrate. A first-order transition can occur if separate domains of each species coexist on the substrate at the same spreading pressure during the displacement process. Menaucourt and Bockel applied this latter idea to the case of displacement of one pure film by another and successfully predicted the vapor pressure of displacement of SF_6 by Xe.[6] For the case of Kr/CCl_4, the x-ray diffraction results of Abdelmoula *et al.*[1] support this picture of displacement, indicating that the emergence of a pure Kr monolayer structure is accompanied by a diminishing of the pure CCl_4 monolayer domain and the simultaneous emergence of a diffraction signal indicative of bulk CCl_4 crystal growth.

Using this qualitative picture of displacement, we recently presented a simple and general thermodynamic description of displacement accommodating any displacement of a saturated preadsorbate monolayer (to be called species 1) that results in a pure film of the inert gas (species 2), by either first-order or continuous processes.[12] For first-order displacement, domains of (or rich in) species 1 and 2 coexist, as separate phases sharing a unique spreading pressure ϕ, until the species 2 phase has completely replaced that of species 1. In continuous displacement, a single phase mixed film is formed, with displacement occurring continuously as the concentration of species 2 in the solution runs from 0 to 100%. A simple thermodynamic relation applies to both types of displacement, given (1) the coexistence with bulk crystals of species 1, fixing the chemical potential μ_1 at the bulk saturated value μ_1^0 and (2) that, at some inert gas chemical potential μ_2^{disp}, displacement of the preadsorbate becomes complete, resulting in a pure film of species 2 identical to that formed in the absence of species 1. In this limit, one can relate the equations of state for the inert gas film density in single species adsorption n_2^{ss} and in the coadsorbed film n_2^{coad} with the saturated spreading pressure of the preadsorbate ϕ_1^0

$$\int_{-\infty}^{\mu_2^{\mathrm{disp}}} (n_2^{\mathrm{ss}} - n_2^{\mathrm{coad}})\, d\mu_2' = \phi_1^0(T). \tag{1}$$

As $\phi_1^0(T)$ is a property of the preadsorbate itself, independent of the second adsorbate, the integral on the left hand side of Eq. (1) should thus be the same for two different inert gases displacing the same preadsorbate. Equation (1) thus expresses an experimentally verifiable prediction of this simple model for coadsorption systems exhibiting displace-

ment. The left-hand side of Eq. (1) can be evaluated by integrating measured isotherm data and is precisely the area between the coadsorption and single species isotherm curves, as plotted, for example, in Fig. 4 below. The limit of species 1 saturation is approached experimentally by ''overfilling'' the cell with several monolayers worth of the preadsorbate to ensure the creation of bulk crystals. Comparison of coadsorption and single species isotherm data can reveal the extent to which displacement runs to completion, resulting in a pure film of the second adsorbate.

Such a comparison was performed for CCl_4 using the Kr/CCl_4 and CH_4/CCl_4 coadsorption systems, working in the limit of $\mu_{CCl_4}=\mu^0_{CCl_4}$, with excess fillings of CCl_4 and measured simultaneously in the same cryostat with the calorimetric data presented here. Measurements for the two systems yielded the same value for $\phi^0_{CCl_4}$ at the level of a few percent across the temperature range of 77 to 112 K, in confirmation of the equilibrium thermodynamic model of displacement.

The applicability of equilibrium thermodynamics in describing displacement is in a sense surprising, given the low vapor pressure of CCl_4, and, indeed, not all aspects of the Kr/CCl_4 coadsorption system are described well by an equilibrium model. The low CCl_4 saturated vapor pressure at low temperatures essentially ''freezes out'' the exchange of the preadsorbate molecules with the gas phase and thus restricts the CCl_4 mobility to surface diffusion processes. The Kr/CCl_4 studies cited here[1,2,12] all report varying degrees of incompleteness of the displacement of CCl_4, with a substantial fraction of the surface area remaining covered by CCl_4. This is consistent with the idea that slow kinetics prevent formation of the true equilibrium macroscopic CCl_4 crystals that would free nearly the entire graphite surface for adsorption by the displacing Kr film.

It should also be noted, however, that the lack of a global equilibrium with the gas phase does not preclude the existence of local equilibrium between CCl_4 film, CCl_4 bulk, and Kr or Kr/CCl_4 film phases, which come in close contact on the graphite substrate. Whether or not molecules are exchanged through the vapor phase, the CCl_4 film is still unstable to 3D crystal growth at the chemical potential fixed by bulk solid CCl_4 in the cell, which is nearly independent of the pressure imposed by the vapor phase. Stated differently, a CCl_4 film still becomes unstable to displacement, mechanically as well as thermodynamically, in the presence of another possible film phase of spreading pressure higher than $\phi^0_{CCl_4}$. As such, the local equilibrium picture can be relevant even without a global equilibrium, permitting creation of bulk solid CCl_4 in coexistence with monolayer CCl_4. This is consistent both with observed x-ray evidence[1] for creation of 3D CCl_4 crystals following displacement by Kr and the experimental measurements of $\phi^0_{CCl_4}$ by Kr and CH_4 displacement.[12] As the exact nature of the crystals formed by displacement and their exact chemical potential are not known, the $\phi^0_{CCl_4}(T)$ relevant in the thermodynamic model can differ slightly from the true bulk solid equilibrium value. Equilibrium in the Kr/CCl_4 coadsorption system will be revisited in both the discussion of the experimental technique (Sec. III) and in the concluding comments (Sec. V B).

The Abdelmoula *et al.*, study[1] of Kr/CCl_4 at 80 K reported CCl_4 displacement as a first-order transition, with no evidence for formation of a mixed Kr/CCl_4 film. Our volumetric study[12], extending above 110 K, however, showed displacement of CCl_4 in a continuous process, occurring over an increasingly wide range of Kr chemical potential with increasing temperature. The graphite substrate used in our study is roughly 20 times denser than that used by Abdelmoula *et al.*, and has a reduced degree of surface uniformity, which has been observed to produce ''broadening'' of the displacement transition (see, for instance, Ref. 2) and likely explains the slight broadening of the displacement transition observed even at the lowest temperatures of our study.[12] However, it cannot explain the temperature dependence observed here, nor the large, order of magnitude, pressure range over which displacement is observed at the high temperature end of the study. The continuous nature of the transition at higher temperatures carries the thermodynamic implication that displacement is occurring in a single phase,[13] mixed Kr/CCl_4, process, rather than a first-order phase coexistence of separate CCl_4 and Kr domains. Mixing in coadsorbed films has been studied theoretically in the context of displacement,[14] though direct observation of solution phases has not been observed in the experimental studies of Kr/CCl_4. Our observation of continuous displacement helped to motivate both the general thermodynamic model of displacement discussed above and the detailed calorimetric exploration of the Kr/CCl_4 coadsorption phase diagram presented in this paper.

While not exhibiting the surface uniformity offered by the most expanded versions of exfoliated graphite, the more compressed graphite substrate we use has the virtue of a greatly increased surface area. The increased amount of adsorbate thus contained in a film of given thickness makes calorimetry an effective probe of the film structure, with phase transitions occurring in single layers of film giving rise to detectable heat capacity signals. In this study, we use calorimetry to detect phase boundaries in the Kr/CCl_4 coadsorption system. Comparison with similar calorimetry data for pure Kr on bare graphite, measured in the same cryostat,[15,16], allows a test of the purity of the Kr film formed by displacement and a search for unique characteristics of the coadsorption system, associated with displacement itself or with possible mixture phases. Combining the calorimetric data with previously presented volumetric equation of state data[12] allows construction of the Kr/CCl_4 coadsorption phase diagram between 77 and 130 K and for films up to four layers thick. These calorimetric data are discussed in detail in Sec. IV. While another wide temperature range study, using x-ray diffraction, discovered a range of interesting phenomena, including displacement and mixing, in the Kr/SF_6 system,[9] the comprehensive and highly resolved thermodynamic investigation of Kr/CCl_4 presented here is a unique contribution in the field of coadsorption and displacement.

A final motivation of this study is to extend the phase diagram for pure Kr on graphite to thicker film coverages.

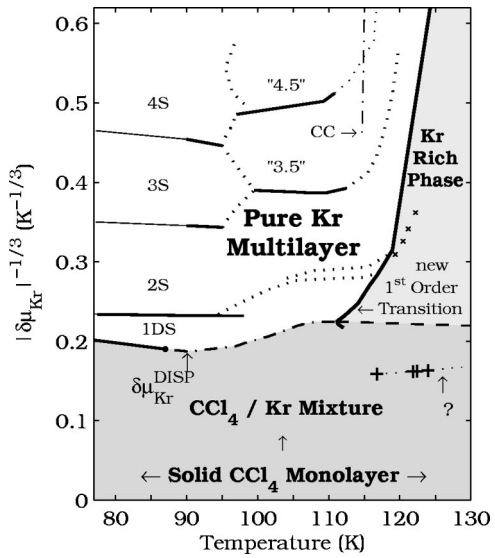

FIG. 1. Proposed phase diagram for coadsorption of Kr and CCl_4, for $\delta\mu_{CCl_4}=0$

Studies of noble gas films in our apparatus had been limited to coverages of several layers of film, with the study of thicker films prevented by the onset of capillary condensation.[15,17–19] The nucleation of the bulk phase in the abundant small pores of the Grafoam substrate not only competes with film growth, but its melting produces a large latent heat signal near the bulk triple point, which obscures important signals arising from phase transitions in the thickening film. The problem is vexing because experiments on multilayer Kr films near the bulk triple point could open a window on the phases of matter near a bulk surface and on the melting transition in the evolution from a two-dimensional film into bulk condensed matter. This is particularly true in light of observed novel reentrant layering phenomena in several-layer-thick noble gas films on graphite,[20] which has been interpreted as the onset of the ''preroughened'' disordered-flat phase of a bulk solid-gas interface[15,21] and, alternatively, as a surface layer melting phenomenon,[22] with recent studies focusing on the possible connection between preroughening and surface layer melting.[23,24] By overfilling the graphite substrate with the nonwetting CCl_4, one can hope to occupy the pores with the preadsorbate, inhibit the growth of Kr capillary condensation, and, should Kr displace the preadsorbed monolayer film, allow for a study of thicker Kr films on graphite. This study of coadsorbed Kr/CCl_4 allowed a modest extension of the ''thick'' Kr film phase diagram and this contribution will be discussed in Sec. IV D.

II. OVERVIEW OF THE PROPOSED Kr/CCl_4 PHASE DIAGRAM

We begin by summarizing the proposed phase diagram for Kr/CCl_4 coadsorbed on graphite, as shown in Fig. 1, before discussing the experimental technique (Sec. III) and results (Sec. IV) used to draw these conclusions. The coadsorption phase diagram is plotted in the $(T,|\delta\mu_{Kr}|^{-1/3})$ plane, where T is temperature and $\delta\mu_{Kr}$ $(\equiv\mu_{Kr}-\mu_{Kr}^0)$ is the chemical potential of Kr measured relative to $\mu_{Kr}^0(T)$, the bulk saturated chemical potential. Similar to $\delta\mu_{Kr}$, which approaches zero from below, $|\delta\mu_{Kr}|^{-1/3}$ also increases as the film grows thicker. Because of the inverse cube law of the Van der Waals substrate attraction felt by an adsorbed molecule, $|\delta\mu_{Kr}|^{-1/3}$ is roughly proportional to the adsorbed film thickness[25] and thus conveniently spaces the individual layers in a multilayer film phase diagram such as that shown in Fig. 1. For smaller portions of the phase diagram, we use the more physically intuitive $\delta\mu_{Kr}$ as the ordinate.

Assuming that the CCl_4 chemical potential is fixed at saturation by the presence of bulk solid $(\delta\mu_{CCl_4}\equiv\mu_{CCl_4}-\mu_{CCl_4}^0=0)$, variables T and $\delta\mu_{Kr}$ provide a full thermodynamic description of the system. Choosing to plot the coadsorption phase diagrams in $(T,\delta\mu_{Kr})$, selecting chemical potential instead of number, allows easier comparison to the single species Kr adsorption data and to experiments performed in other apparati, independent of the surface area available to the coadsorbed film, which can depend on the nontrivial distribution of the excess bulk CCl_4.

At the bottom of the coadsorption phase diagram, for $|\delta\mu_{Kr}|^{-1/3}=0$ (equivalently, for $\delta\mu_{Kr}=-\infty$), our experiments begin with a pure saturated monolayer of CCl_4. As Kr is introduced with increasing chemical potential, it adsorbs in continuous fashion into a single phase solution film with CCl_4, with displaced CCl_4 forming bulk solid. Displacement becomes complete at $\delta\mu_{Kr}^{disp}(T)$, where the Kr density in the coadsorption system is observed, in the volumetric coverage measurements, to become equal to that of a pure Kr film. Crossing below this line in a calorimetry experiment, from higher to lower $\delta\mu_{Kr}$, results in a broad heat capacity feature due to the onset of Kr desorption as the film enters a mixed phase, with CCl_4 reversibly reclaiming the graphite surface. The sharp onset of desorption suggests that, although displacement is clearly continuous at such temperatures, with no discontinuous jump in the Kr coverage, passing below the line at $\delta\mu_{Kr}^{disp}(T)$, marked ''-·-,'' does indeed represent a true transition into a mixed film phase.

The displacement transition, shown to be clearly continuous at the higher temperatures in our study, is drawn to be first-order at low temperatures (solid line), in correspondence with the observation of first-order displacement at 80 K by Abdelmoula, *et al.* The speculation of a critical point, roughly placed here at 87 K, is in analogy to the observation of a critical-like displacement transition in Kr/cyclohexane and corresponds to a rough extrapolation of our isotherm slope data. At high temperatures and low Kr coverage in the mixed phase, a small heat capacity feature signifies a new, unidentified phase boundary that indicates some change in the structure of the Kr/CCl_4 mixture (marked + in Fig. 1). Low coverage calorimetry data leading up to displacement completion are discussed in Sec. IV A.

At Kr chemical potentials above $\delta\mu_{Kr}^{disp}(T)$, coadsorption calorimetry data indicate that a pure Kr multilayer forms on the bare graphite surface, with a phase diagram identical to that of single species Kr adsorption. Just as the first-order layering transitions from one to two and then three layers of

film are observed as vertical steps in the coadsorbed coverage data, so are the heat capacity features, marking triple points, melting curves, critical points, and commensurability transitions, reproduced along the same phase boundaries observed for single species Kr adsorption. This evidence for the creation of a pure Kr film confirms this assumption of the thermodynamic model of displacement discussed in the introduction and presented previously.[12] Discussion of the pure Kr film formed by displacement can be found in Sec. IV B.

Within the realm of this pure Kr multilayer, at high Kr coverages in the coadsorption system one finds evidence of the nucleation and melting of unsaturated Kr capillary condensate, along the line labeled ''CC.'' However, because the smaller pores are effectively filled with the preadsorbed CCl_4, the onset of this feature is delayed to higher Kr coverage than observed in the single species Kr adsorption system, permitting study of thicker multilayer Kr films. This permits clearer observations of a continuous extension of the reentrant first-order layering transition between densities of roughly 2.5 and 3.5 layers and the first evidence for a similar extension of the 3.5–4.5 reentrant layering phase boundary. Data for the thick Kr films is discussed in Sec. IV D.

Above 112 K, a dominant heat capacity feature, with no analog in the pure Kr adsorption system, is observed, representing a first-order phase transition, likely between a pure Kr film and a Kr rich mixture phase. This phase, marked in light gray in the phase diagram, has a lower Kr density than the pure Kr phase, with a density discontinuity of as much as 10% upon crossing the first-order phase boundary. At these temperatures, there is still a sharp onset of desorption upon crossing a boundary, marked ''- -,'' that extends from the lower temperature displacement completion line. However, coadsorption isotherm measurements indicate that the film only reaches the pure Kr density upon crossing the first-order phase boundary, which we thus associate with the completion of displacement at these higher temperatures. Section IV C presents this new transition unique to the Kr/CCl_4 coadsorption system.

III. EXPERIMENTAL TECHNIQUE

Measurements were performed with an automated scanning ratio calorimeter, which was designed specifically for the detection of phase transitions in thin adsorbed films on graphite and permits continuous measurement of film heat capacity and vapor pressure while scanning across a wide temperature range. The adsorption cell consists of 29 g of Grafoam[26] in a volume of roughly 100 cc, and the $\sqrt{3}\times\sqrt{3}$ coverage commensurate with the graphite lattice has been determined to be $N_{\sqrt{3}}=165$ stpcc.[15,27]. During measurement, the cell temperature is controlled to equal that of a copper block standard, which is steadily heated through the temperature range of interest. Heat capacity data are then extracted from the cell heater signal. The sample cell is connected to a room temperature barocell, allowing simultaneous measurement of the film vapor pressure. Note that for the temperature range of this study, the saturated vapor pressure of CCl_4 is orders of magnitude lower than that of a Kr film. Thus, the measured vapor pressure is very nearly that of the Kr film and permits an accurate calculation of the Kr chemical potential $\delta\mu_{Kr}$ and, by volumetric analysis, film coverage, N_{Kr}. Full details of the design and operation of the calorimeter have been presented elsewhere,[27,28] and we highlight here the procedures specific to the coadsorption experiments.

A. Preadsorbed film preparation and cooldown

The aim in preparing the preadsorbate film is to grow a uniform and complete monolayer film of CCl_4 in conditions as close as possible to equilibrium, with excess CCl_4 forming bulk solid in the pores of the graphite substrate. Growing the equilibrium low temperature film is complicated by the low CCl_4 saturated vapor pressure, extrapolated to lie between roughly 10^{-20} and 10^{-8} Torr in our 75–130 K range of study,[1] which effectively prevents exchange of molecules with the gas phase on experimental time scales. Here, as in other coadsorption studies[1] with CCl_4, the idea is to introduce the preadsorbate at higher temperatures, where equilibrium times are relatively quick, and then cool slowly to liquid nitrogen temperatures, limiting temperature gradients or other disturbances that could allow the CCl_4 to ''freeze'' into a nonequilibrium state.

It is important to note that the equilibrium film phase of CCl_4 on graphite at saturated vapor pressure is a solid monolayer at temperatures below 217 K. This was identified by Abdelmoula *et al.*[11] as the ''dewetting temperature'' for the second layer of a bilayer solid that is the stable film at bulk saturation between 217 and 235 K.[10] The incommensurate monolayer $\sqrt{3}\times\sqrt{3}$ structure observed below 217 K persists down to liquid nitrogen temperatures. As such, up to the relatively warm temperature of 217 K, where the vapor pressure is a fraction of 1 Torr and film-gas equilibration is achieved quickly, the film can be prepared into a state similar to that of the low temperature equilibrium film.

The data presented in this paper were measured on four different coadsorption cooldowns, labeled A–D, each with the cell loaded at room temperature with CCl_4, with fillings ranging from five to eight times the monolayer quantity (given the observed low-temperature monolayer crystalline structure of CCl_4,[10] its monolayer coverage should be roughly 82 stpcc with our substrate). Cooldown A, performed with 430 stpcc of CCl_4, served as a first exploration of the coadsorption phase boundaries. Cooldowns B and C, also using 430 stpcc of CCl_4, targeted the precision measurement of the coadsorption film density equations of state from very low coverages through the completion of displacement across the 75–115 K temperature range (the cooldown B isotherm data was presented in Ref. 12). Finally, cooldown D, performed with 600 stpcc CCl_4, aimed specifically at extending our previous ''thick film'' pure Kr measurements by suppressing the Kr capillary condensate with CCl_4. The film preparation procedures, which were improved with each cooldown, are discussed in detail elsewhere,[29] as are the measurement and data analysis techniques.

Cooldowns were performed over several days and interrupted at intermediate temperatures where the CCl_4 vapor pressure was sufficient to test that it condensed in the cell rather than at other stages along the fill tube. Even cooling

down slowly, we found, in cooldowns A and B, a large impedance to gas flow in and out of the cell, resulting in times of up to an hour for Kr gas to reach the cell, indicating formation of a partial CCl_4 plug at the entrance to the graphite cell. The resultant slowed pressure equilibration necessitated a slight correction to the measured pressure data, which is discussed in the next subsection.

The problem of the partially plugged cell was solved in cooldowns C and D by interrupting the cooldown near 205 K, where the roughly 0.1 Torr saturated vapor pressure is still high enough for measurement and relatively quick evaporation of any CCl_4 frozen outside the cell. Control and modulation of the temperature of all stages, combined with patient monitoring of the vapor pressure, allowed both evaporation of any bulk CCl_4 condensed and a verification that only the graphite cell contained CCl_4 in significant quantity. Additionally, the vapor pressure was measured to be within 10% (roughly the absolute gauge accuracy in this pressure range) of the saturated value calculated from the published values data.[11] As stated above, observing equilibrium conditions at such intermediate temperatures means that the film is already near the equilibrium low temperature configuration. Continuing the cooldown, with the vapor pressure becoming too low for precise determination of the CCl_4 relative saturation, the apparatus was cooled at several degrees per hour to liquid nitrogen temperature. The cell was always maintained several degrees colder than the other stages along the fill tube in order to prevent migration of the preadsorbate out of the graphite substrate. Observing the pressure upon low temperature admission of bursts of He gas into the cell allowed verification that flow into the cell was not impeded and allowed calibration of the free volume of the cell.

Following cooldown to liquid nitrogen temperatures, introduction of the first small dose of Kr to the graphite substrate allowed evaluation of the completeness of the adsorbed CCl_4 film. The ratio of the amount of Kr adsorbed to the amount of Kr adsorbed at the same temperature and vapor pressure in the pure Kr film places a limit on the percentage of the substrate left bare. This is an upper limit, because Kr can also adsorb on top of, or dissolve into, the CCl_4 film. For cooldowns B and C, used for precision measurement of the coadsorption equation of state, this ratio indicates that no more than 2% of the graphite surface was left bare, and so the coadsorption experiments were truly performed in the limit of a full CCl_4 monolayer with excess CCl_4 condensed in the cell.

Even with the controlled cooldown procedure, several observations indicate that the CCl_4 does not reach a reproducible equilibrium state in the distribution of crystals formed in the cooldown and by displacement. First, there is the already mentioned reduction in the surface area which the Kr film occupies adsorbs following displacement, determined to be roughly 63 and 48%, respectively, of the full surface area in the cooldowns B and C. This results in the need to normalize coverages with respect to the surface area available for coadsorption, requiring a scale factor F, which varied between the different cooldowns and will be described in the next subsection, to normalize properly the film density calculations using the amount of Kr adsorbed at displacement completion. Second, the effective volume of the cell is also observed to be reduced, by 20 to 30%, after CCl_4 adsorption, indicating that a small portion of the cell can be effectively sealed off by frozen CCl_4. That a relatively small amount of CCl_4, which condenses into a volume of several cm^3, can block off a significant portion of a cell with 100 cc free volume and occupy a significant portion of its surface area is clear evidence that the CCl_4 does not all condense as capillary condensate in the pores of the system or as macroscopic bulk crystals as one would expect from equilibrium considerations.

In light of the evidence for a non-reproducible distribution of the excess bulk CCl_4, a few words should be said here on the reproducibility of the coadsorbed film measurements that follow the preadsorbate cooldown. First, the location of the heat capacity maxima in $(T, \delta\mu_{Kr})$ plotted together for all the cooldowns in Fig. 3 and used to determine the coadsorption system phase boundaries, are consistently reproduced in all four cooldowns. There is a slight broadening of peaks in the first two cooldowns with respect to those of the final two, likely due to the delays in gas flow in and out of the cell discussed above. However, the measured phase boundaries are in agreement with those in the final two cooldowns. Secondly, the coadsorbed Kr equation of state measurements, are reproduced to high accuracy in cooldowns B and C, as seen by the overlap in the coadsorption isotherm data in Fig. 4, in spite of significant differences in the cooldown procedure and in the resulting amounts of surface area ''lost'' to the excess CCl_4. As such, the irreproducibility in the distribution of the excess condensed bulk CCl_4, does not have a measurable effect on the thermodynamic properties of the coadsorbed Kr/CCl_4 film, which are the main focus of this study. This is consistent with the thermodynamic picture of a bulk CCl_4 phase fixing the preadsorbate chemical potential in the experiments.

B. Coadsorbed film preparation, measurement, and analysis

Coadsorbed films were formed by the addition of small doses of Kr, typically on the order of 10% of a monolayer, to the cell. To obtain reliable film coverage data, in particular for cooldowns B and C, where we have used the entire datasets to construct coadsorption isotherms, measurement runs were performed in order of increasing Kr coverage. Keeping the system on the ''adsorption branch'' of film growth by monotonically increasing the Kr coverage limits the film coverage hysteresis due to the nucleation, and subsequent evaporation, of capillary condensate, as is known to occur in film systems subject to cycles of adsorption and desorption.[19] After ''annealing'' the system at the high temperature end of the study, the films were cooled and then warmed across the temperature range of interest. Heat capacity data were recorded continuously on the warming cycle, while scanning at approximately 2 K/h across a temperature range of 10–50 K.

Pressure data, which permit calculation of the Kr chemical potential, were recorded on both the cooling and warming cycles, as illustrated for several runs from cooldown C in

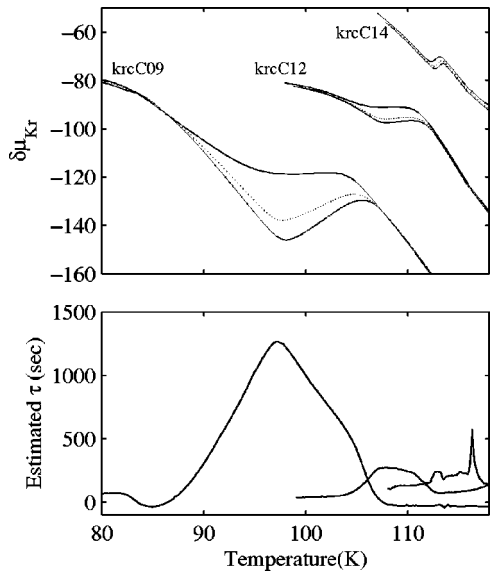

FIG. 2. Cooling (upper solid curve) and heating (lower solid) chemical potential trajectories for several ''C cooldown'' runs, plotted with the estimated equilibrium trajectories (dotted curves). The lower plot shows, for the same runs, the estimated film-vapor equilibration times.

Fig. 2. A finite gas-film equilibration time leads to the opening of a hysteretic loop in between the heating and cooling data, which becomes significant in the region of $(T,\delta\mu_{\mathrm{Kr}})$ that will be shown to be characterized by the transport of CCl_4, which means, upon cooling, being displaced from the monolayer film state or, upon heating, reentering the film phase. Importantly, note that at both the hot and cold extremes of the runs, the hysteresis between the heating and cooling legs closes, meaning that all Kr adsorption (and thus any corresponding CCl_4 displacement) occurring on the cooling cycle is reversibly undone on the heating cycle, the film returning to its original coverage and chemical potential. As such, the CCl_4, in spite of its low vapor pressure, does manage to move in and out of the film on the time scales of the experiment.

In order to correct for the time lag in the dynamic measurement of the film vapor pressure, we assume a simple linear equilibration model for the film vapor pressure p,

$$\frac{dp}{dt} = -\frac{p - p_0(T,n_{\mathrm{Kr}})}{\tau(T,n_{\mathrm{Kr}})}. \tag{2}$$

Using Eq. (2), we can combine the cooling and warming data for the pressure and the pressure time derivative to estimate the film's equilibrium vapor pressure p_0 and characteristic equilibration time τ for a given temperature T and Kr film density n_{Kr}. Several such equilibrium curves, for the calculated chemical potential, are shown in dotted lines in Fig. 2, naturally falling between the heating and cooling data. This dynamic estimate for $p_0(T)$ was compared in several cases with that measured with the cell temperature fixed, upon interruption of both the heating and cooling cycles. These were performed in the ''worst case'' cooldown B, in which the equilibration times were significantly lengthened, particularly at low temperature and pressure, by the previously mentioned partial blockage of the fill tube. The computed values for μ_{Kr} were found to agree within 10 K at the lowest temperatures, while above 90 K, where this study reveals most about the coadsorption phase diagram, the agreement was within 1 K, quite small in comparison with the relevant temperature and energy scales in the system.

The lower portion of Fig. 2 illustrates the corresponding estimated equilibrium times for the same three cooldown C runs. This is valid only in giving an idea of the longer equilibration times, which can be seen to be roughly a half hour during the displacement process (see the data for run krcC09 between 95 and 105 K). For the shorter equilibration times, the sensitivity to the very small differences in the cooling and heating data makes the equilibrium time estimate unreliable (the feature in the krcC14 equilibrium time data around 118 K corresponds to small artifacts in the pressure data, magnified by the proximity of the heating/cooling curves). However, also because the heating and cooling curves are close in these cases, the error in the equilibration time estimate introduces no significant error in calculating the corresponding equilibrium pressure and chemical potential.

The observed timescale, less than an hour, for equilibrium during the displacement process, as the system passes through the region of $(T,\delta\mu_{\mathrm{Kr}})$ below the displacement completion line (as in krcC09), is far too short to be explained by exchange of CCl_4 molecules between the film and gas phases. The lack of equilibrium between CCl_4 film and gas phases on experimental time scales, due to its low saturation vapor pressure, has already been mentioned. A simple balance between gas molecules striking the adsorption substrate and film molecules desorbing into the gas phase[30] gives an expected ''sticking time,'' characterizing the CCl_4 film-gas equilibrium, of order several months at 100 K. As such, the relatively quick transport of CCl_4 between film and bulk phases during displacement must involve surface diffusion processes, rather than the film-gas exchange that can permit quick equilibrium in a pure Kr film at the same temperatures. A final ''thermal transpiration'' correction,[31] relevant only at the lowest temperatures and pressures of the study, was applied to the pressure data and corrects for the thermal gradient between the cell and the pressure gauge.

For each Kr filling, a run thus yields, as a function of T, the system heat capacity C and vapor pressure p. The latter allows calculation of the Kr chemical potential, $\delta\mu_{\mathrm{Kr}}$, and, by volumetric subtraction of the number of atoms in the gas phase, the number in the film $N_{\mathrm{Kr}}^{\mathrm{film}}$. When plotted in this paper, runs from the four coadsorption cooldowns are labeled ''krcA'' through ''krcD,'' c implying coadsorption (when shown for comparison, data measured for pure Kr on graphite are labeled ''krsA,'' s indicating single species Kr adsorption). Where given, the nominal run coverages (the total amount of Kr, in both condensed and gas phases) and the actual amount condensed on the substrate are expressed in units of $\sqrt{3}\times\sqrt{3}$ monolayers and have been normalized to the surface area available for Kr adsorption, a correction to be discussed shortly.

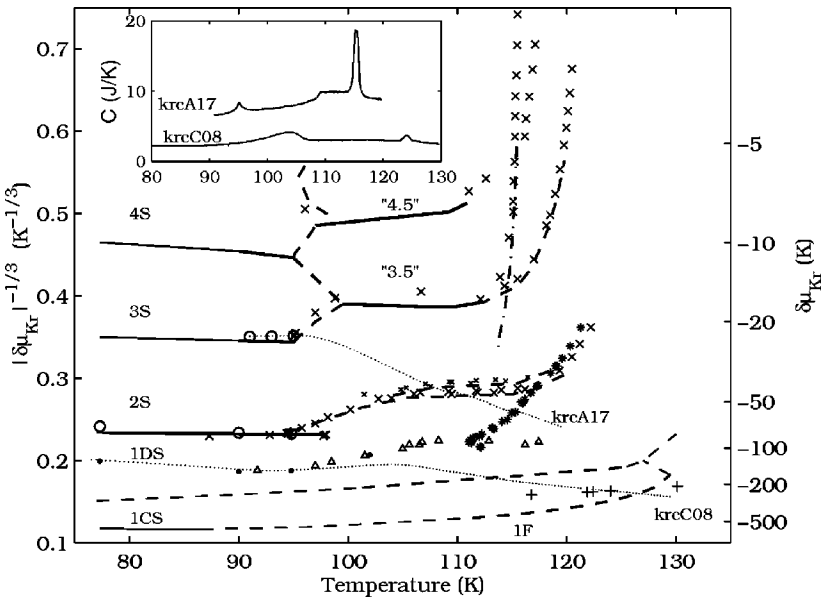

FIG. 3. Kr/CCl_4 phase boundary crossings, plotted against the multilayer phase diagram for Kr on bare graphite (solid and dashed lines). The pure Kr phase diagram presented here was measured in the same cryostat used for this coadsorption study (Refs. 15 and 16), supplemented by extensions, drawn with a thinner line weight, in the monolayer regime and at low temperatures, based on other published experimental data (Refs. 32–34). Solid lines at lower temperatures represent first-order layering transitions, growing from one (''1DS'') to two (''2S'') to three (''3S'') solid monolayers and so on. The first layer has solid phases that are commensurate (''1CS'') and dense (''1DS'') with respect to the $\sqrt{3}\times\sqrt{3}$ graphite lattice, in addition to a single fluid phase (''1F'') (Refs. 32,33). The second layer, instead, has triple and critical layering points, at 95 and 98 K, with a melting line extending to high temperatures (marked ''–,'' as for other apparently continuous transitions), where it is accompanied closely by another phase boundary, likely a commensurability transition. The upper layers feature a reemergence of first-order layering at temperatures above 100 K, resulting in roughly half-integer coverages (''3.5,''''4.5''), with this novel reentrant layering ''zippered'' to the lower temperature first-order layering transitions by a series of continuous transitions (Refs. 20,21). Finally, the phase boundary, marked ''-··-,'' leading to the 116 K bulk Kr triple point has been associated with melting of unsaturated capillary condensate (Ref. 19). For the Kr/CCl_4 coadsorption data, heat capacity features that resemble those found for pure Kr are marked $\times$. A new first-order phase boundary unique to coadsorption, associated with a large heat capacity peak, is plotted as *, while an unidentified low coverage feature is marked $+$. The onset of a broad desorption figure is marked $\triangle$. From the equation of state measurements, we identify first-order layering transitions with $\bigcirc$ and the point at which the coadsorption isotherm curves join the pure Kr data with $\bullet$. ''Experimental trajectory'' curves traced across the phase diagram by two sample runs are also plotted with dotted lines (krcC08 and krcA17, with 1.25 and 3.31 $\sqrt{3}\times\sqrt{3}$ monolayers), as well as the corresponding heat capacity data (inset). Locating the heat capacity maxima, in $(T,\delta\mu_{Kr})$, for such runs is essential in identifying phase boundaries.

Identifying peaks and other features in the heat capacity data is our primary tool in constructing the Kr/CCl_4 coadsorption phase diagram. Figure 3 shows the location in $(T,\delta\mu_{Kr})$ of such heat capacity and film coverage anomalies, plotted against the phase boundaries measured for Kr single species adsorption on graphite, as presented in Refs. 15,16. The meanings of the various markers are given in the caption and will be discussed in detail in the next section. The heat capacity data (inset) and chemical potential ''trajectories'' for two typical runs are also shown in this figure, illustrating that the temperatures of various heat capacity features are marked along the curves in $(T,\delta\mu_{Kr})$ to signify the crossing of a candidate phase boundary.

Another clue to the state of the film at a given point in the $(T,\delta\mu_{Kr})$ plane is provided by the film coverage data, which, for a series of runs at different Kr coverages, can be ''sliced'' at various temperatures to form a set of isotherms. Figure 4 displays coadsorption isotherms made at several different temperatures, plotted against the corresponding single species isotherm data. This also illustrates the overlap between data taken on two different cooldowns. For each cooldown, the film density n_{Kr} in units of $\sqrt{3}\times\sqrt{3}$ monolayers, has been computed using a surface area normalization factor F needed to overlap the ''post-displacement'' coadsorption isotherm data with the pure Kr isotherms

$$n_{Kr}=\frac{N_{Kr}^{film}}{N_{\sqrt{3}}}F. \tag{3}$$

F^{-1} represents the fraction of the substrate area available for film growth. For the data of a given cooldown, F varied between cooldowns (between 1.2 and 2.1) depending on the amount of CCl_4 used and on the success in condensing all the preadsorbate inside the sample cell. However, F was found to be consistent across the temperature range studied for a given cooldown, indicating that F is a relevant indicator of the available surface area, which remains constant in a given cooldown. Likewise, the resultant coadsorption film densities, n_{Kr}, were reproducible between cooldowns, as seen in the overlap of the coadsorption isotherms in Fig. 4. The reduction in the available surface area for coadsorption

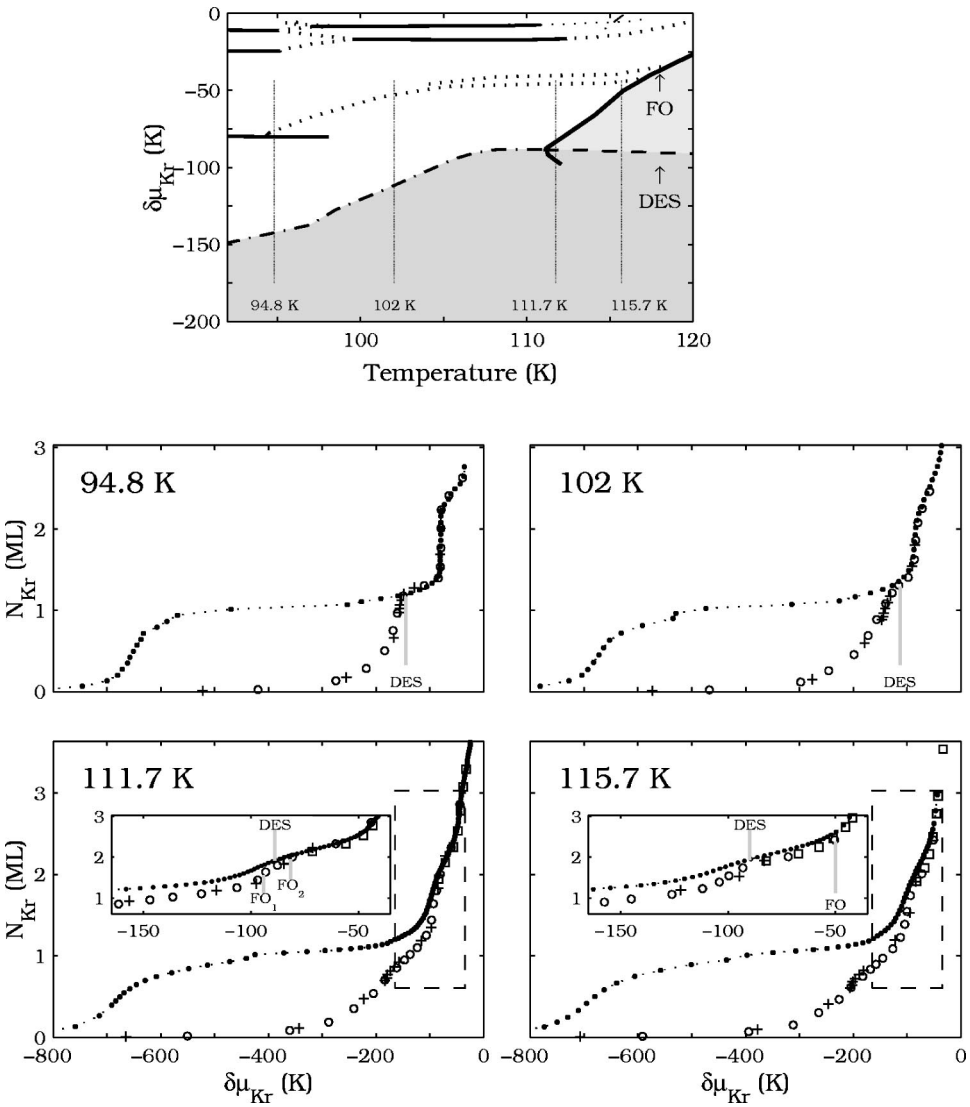

FIG. 4. Single species (●) and coadsorption (from cooldowns B, marked ○, and C, marked +) isotherm data at 94.8, 102, 111.7, and 115.7 K. Coadsorption data from cooldown A has also been used (marked with squares) in the two higher temperature isotherms to extend to higher Kr coverages (Ref. 35). A scale factor F equal to 1.21, 1.60, and 2.10 has been employed, respectively, for cooldowns A, B, and C. The schematic figure at the top shows the portions of the phase diagram ''sliced'' by these isotherms. In the isotherm data, the lines marked ''des'' and ''FO'' designate the values of $\delta\mu_{\mathrm{Kr}}(T)$ at which one finds heat capacity features associated with, respectively, the onset of desorption upon entering into a mixed film phase and a new first-order phase transition characteristic of coadsorption.

has been observed, to varying degrees, in all the volumetric studies cited here, and F is discussed in more detail elsewhere.[12,29] While Kr/CCl_4 coadsorption isotherm data were presented in our previous study,[12], they are essential here in the interpretation and construction of the coadsorption phase diagrams, permitting the identification of displacement completion and layering transitions, which are also marked in Fig. 3.

IV. EXPERIMENTAL RESULTS AND DISCUSSION

A. Low Kr coverages: Displacement and desorption

Figure 5 plots coadsorption calorimetry and chemical potential traces for several runs made at low Kr coverage. A broad heat capacity feature, not observed in the data for single species Kr adsorption, appears first in krcC03 (peaking near 98 K), and moves to higher temperatures (104 K in krcC08) with increasing coverage. The peak grows larger and displays a sharper onset at the low temperature side, for example, at 97 K in krcC09, 105 K in krcC11, and 107 K in krcC12. The locations of this ''sharp onset,'' in $(T,\delta\mu_{\mathrm{Kr}})$, can be quantified by the maxima in the second temperature derivative of the heat capacity, where the slope of the calorimetry data increases most rapidly, and are marked △ in Fig. 3.

There is a strong overlap between the onset of this broad heat capacity feature and those, marked ● in Fig. 3, which indicate the completion of displacement, defined as the chemical potential $\delta\mu_{\mathrm{Kr}}^{\mathrm{disp}}$ at which the coadsorption and single species Kr film densities become equal within the experimental uncertainties. The coincidence of these features is also clear from the isotherm data at 95 and 102 K shown in Fig. 4. Here, the label ''des'' marks the values of $\delta\mu_{\mathrm{Kr}}$ at which the curve, in $(T,\delta\mu_{\mathrm{Kr}})$ drawn through the points corresponding to the onset of the broad desorption feature crosses the relevant isotherm temperature (''des'' refers to ''desorption'' for reasons to be explained shortly). Because of this close coincidence between displacement completion and the low T beginning of the broad heat capacity peak, these features (marked ● and △ in Fig. 3) are linked together to form the displacement completion phase boundary, marked ''-·-'' in the proposed phase diagram (Fig. 1).

This broad heat capacity is due in large part to the enhanced rate of Kr desorption as a calorimetry scan crosses

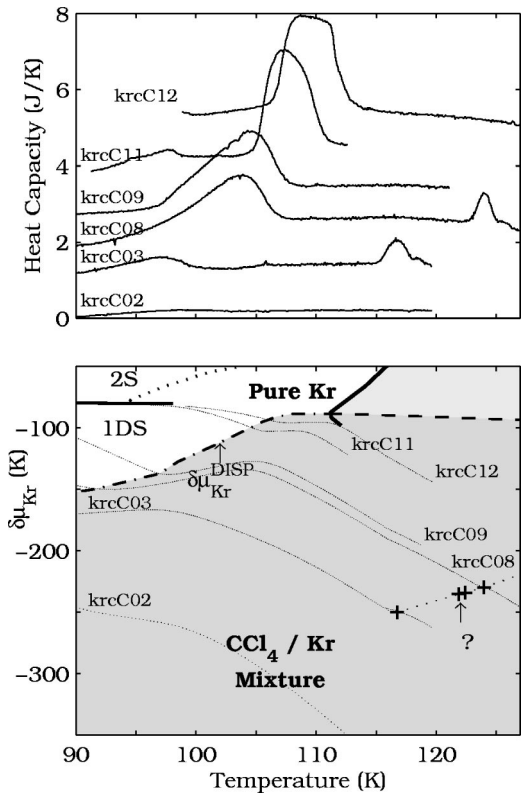

FIG. 5. Low coverage calorimetry and experimental trajectory data for Kr/CCl_4. Runs krcC02, 3, 8, 9, 11, 12, have nominal normalized coverages of 0.19, 0.70, 1.25, 1.34, 1.78, and 2.05 $\sqrt{3} \times \sqrt{3}$ layers.

the phase boundary of displacement completion. As the trajectories plotted in Fig. 5 cross below the displacement completion line, the system enters the dark gray region, labeled "CCl_4/Kr mixture," where isotherm data show the Kr density to be lower than it would be at the same values of $(T, \delta\mu_{\mathrm{Kr}})$ in the absence of CCl_4. Moving to higher T and following a general trend towards lower $\delta\mu_{\mathrm{Kr}}$, displacement is run continuously in reverse, with Kr beginning to move from the film into the gas and CCl_4 leaving the bulk solid phase to reoccupy the surface, "dissolving" into a Kr-rich solution film. The experimental trajectories shown in Fig. 5

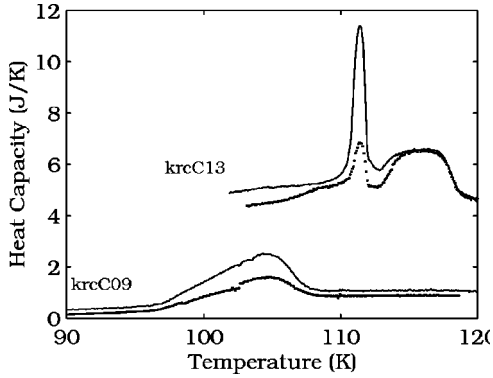

FIG. 6. Heat capacity, total (solid) and that due to desorption (dotted), for coadsorbed Kr/CCl_4.

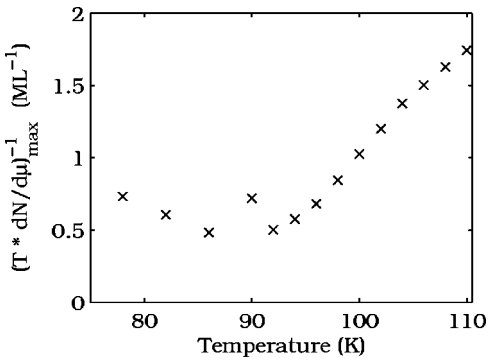

FIG. 7. Plot of the reciprocal isotherm slope showing decreasing slope with increasing temperature, and thus displacement over a broader range of $\delta\mu_{\mathrm{Kr}}$.

all turn briefly towards higher chemical potential upon being heated across the displacement completion line (see, for example, krcC09 near 97 K and krcC12 near 105 K). The turn towards higher $\delta\mu_{\mathrm{Kr}}$ means higher gas pressures and thus an increased rate of Kr desorption upon moving into the mixed film phase below $\delta\mu_{\mathrm{Kr}}^{\mathrm{disp}}(T)$.

Because of the energy required to move Kr from "bound" film sites into the gas phase, the enhanced rate of Kr desorption results in an enhancement of the system heat capacity measured by our calorimeter. This heat capacity enhancement is proportional to the rate of desorption, given by

$$C_{\mathrm{des}} = -T\left[\left(\frac{\partial\mu_F}{\partial T}\right)_{N_F} - \left(\frac{\partial\mu_G}{\partial T}\right)_{N_G}\right]\frac{dN_{\mathrm{Kr}}^{\mathrm{film}}}{dT} \equiv -q_D\frac{dN_{\mathrm{Kr}}^{\mathrm{film}}}{dT}. \quad (4)$$

The heat of desorption q_D can be estimated from our dataset of film coverage as a function of temperature and vapor pressure.[29] Figure 6 plots the total heat capacity and that due to desorption of Kr C_{des} and shows, for the krcC09 run, how a significant portion of the broad heat capacity peak is contributed by this desorption term. Because the desorption term does not completely account for the magnitude of the heat capacity feature, there must be an additional change in the film entropy, some restructuring that accompanies the changing composition of the mixed film phase. Finally, note that although the Kr film densities in Fig. 4 continuously rise to meet the pure Kr isotherm curves, the sharp onset of the broad desorption features seen in Fig. 5 suggests that there may be a higher order phase boundary associated with the completion of displacement. The onset of desorption seen in the heat capacity data, and the possibility that there is a continuous phase transition associated with displacement completion, is likewise reflected in the convergence of the coadsorption and pure Kr isotherm curves at $\delta\mu_{\mathrm{Kr}}^{\mathrm{disp}}$; they do not join with a vertical step in the isotherm data, as one would expect for a first-order displacement transition, but rather meet with a change in slope of the coadsorbed Kr density, as seen most clearly in the 94.8 K isotherm data.

The displacement producing the broad desorption feature is continuous, with Kr adsorption (or desorption) occurring across a wider range of chemical potential as temperature is increased. While Abdelmoula *et al.*,[1] observed first-order displacement of Kr/CCl_4 at 80 K, we do not observe the vertical isotherm step signature of a first-order displacement transition even down to 77 K, likely due to the less uniform surface of our denser substrate. It is qualitatively illustrative, however, to look at the maximum slope of the predisplacement isotherms as a function of temperature, or, as plotted in Fig. 7, at the quantity $(1/T)(dN/d\delta\mu)^{-1}_{\max}$, as has been used in extrapolating to find critical temperatures[7,37] The increase with temperature above 90 K corresponds to the widening range of chemical potentials over which displacement occurs, consistent with a ''supercritical'' displacement phenomenon. At lower temperatures, there is a saturation in the slope, due to the coarse spacing in coverage of our isotherm points as well as any ''washing out'' of a first-order transition due to surface inhomogeneity. The data do not permit a precise measurement of, or even prove the existence of, a critical displacement temperature. However, combining the observation of 80 K first-order displacement,[1] our evidence for continuous displacement at higher temperatures, and a naive fit to the 95–105 K data in Fig. 7, we have speculatively placed a displacement critical point in the neighborhood of 87 K in the proposed phase diagram in Fig. 1. This can clearly be better evaluated by detailed volumetric studies in this temperature range using the more expanded substrates employed by Abdelmoula *et al.*[1]

In addition to the broad desorption feature in the heat capacity data, we observe an additional small heat capacity peak at higher temperatures and lower coverages. Less than 1 J/K in magnitude, this first appears around 117 K in run krcC03 (see Fig. 5), where the Kr density is only 35% of the pure Kr monolayer coverage. The peak is not seen in the krcC02 run at roughly 10% of the monolayer density. The main peak traces out a phase boundary in $(T,\delta\mu_{\mathrm{Kr}})$ that is marked + in Figs. 3 and 5. There is a slight but real bump appearing consistently almost 2 K above the heat capacity maximum, which has been reproduced in a subsequent cooldown, suggesting that there might be two adjacent phase boundaries. While this phase boundary is near, in $(T,\delta\mu_{\mathrm{Kr}})$, those corresponding to monolayer commensurability and melting transitions in the pure Kr system, it does not overlay either of them, and actually crosses the trajectory of the melting boundary from the pure Kr film (compare the relevant coadsorption and pure Kr phase boundaries around 120 K and $\delta\mu_{\mathrm{Kr}}\approx -200$ K in Fig. 3). Furthermore, the size and shape of the peak does not resemble those observed in the pure Kr system.[16,29] As such, this small heat capacity peak can be associated with a transition unique to the coadsorption system. One would not expect to see pure Kr film behavior at these low coverages where the coadsorption isotherm measurements indicate a homogeneous mixed film. While the nature of the phases involved cannot be determined from these thermodynamic measurements, this phase boundary must correspond to some reorganization of the mixed film and raises the possibility that the mixed film may not be fully disordered at these low Kr concentrations. With increasing coverage, this phase boundary runs across the high temperature border of our study.

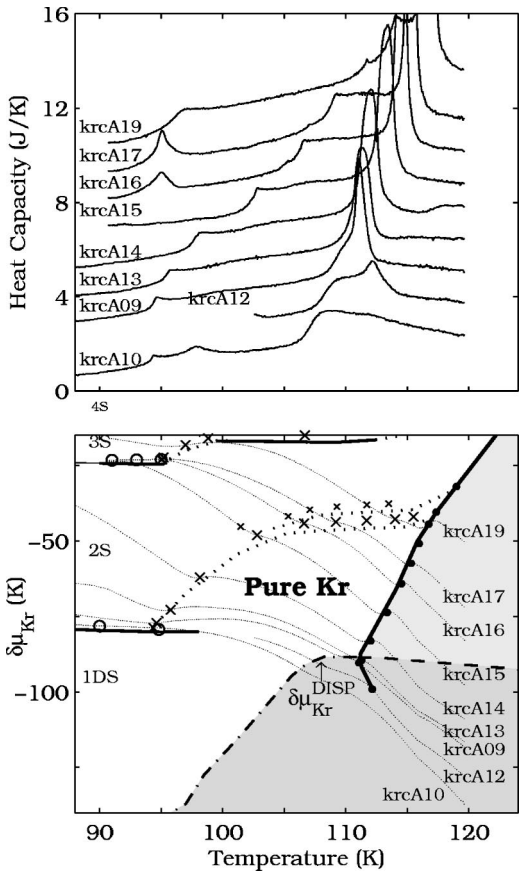

FIG. 8. Heat capacity and chemical potential data for coadsorbed Kr/CCl_4 in the multilayer regime. Runs krcA10, 12, 9, 13, 14, 15, 16, 17, and 19 have approximate nominal normalized coverages of 1.9, 2.0, 2.1, 2.3, 2.5, 2.8, 3.1, 3.3, and 3.9 $\sqrt{3}\times\sqrt{3}$ monolayers. The heat capacity runs are placed in order of increasing coverage, not run number (the cooldown A runs were not all performed in order of increasing coverage).

B. Evidence for a pure Kr film resulting from displacement at low T

Figure 8 displays calorimetry and chemical potential data for a number of coadsorption runs made in the ''post-displacement'' regime of multilayer film growth. A number of small features, beginning near 95 K, closely resemble heat capacity peaks observed for phase transitions in the second and third layer of pure Kr films and trace out phase boundaries that closely overlay the phase diagrams for the higher layers of pure Kr. As such, these data suggest that the multilayer film that results from displacement of CCl_4 is indeed a pure Kr multilayer on bare graphite.

Two small peaks emerge at 95 and 98 K in the krcA10 data, with the lower temperature peak moving to higher temperatures with increased coverage in successive runs. As seen in Fig. 9, these peaks bear strong resemblance in shape and size to peaks from the pure Kr calorimetry dataset.[15] The

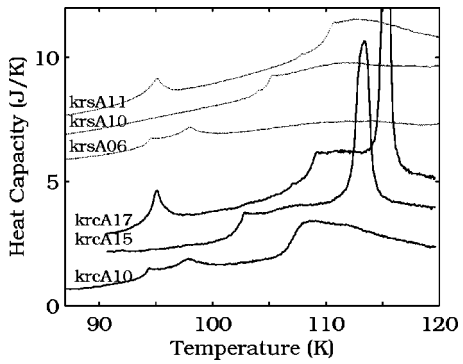

FIG. 9. A comparison of coadsorption (krcA) calorimetry peaks with single species (krsA) film data (Ref. 15) reveals both familiar and new features arising in the Kr/CCl_4 coadsorption system. Common features include second layer melting (95 K in krcA10, 103 K in krcA15, 109 K in krcA17), the second layer critical point (98 K in krcA10), a tiny signal due to a commensurability transition in the second layer (107 K in krcA17), and third layer melting (95 K in krcA17). The larger features peaking at 108, 113, and 116 K in the three krcA runs are unique to the coadsorption system and are discussed in Sec. IV C.

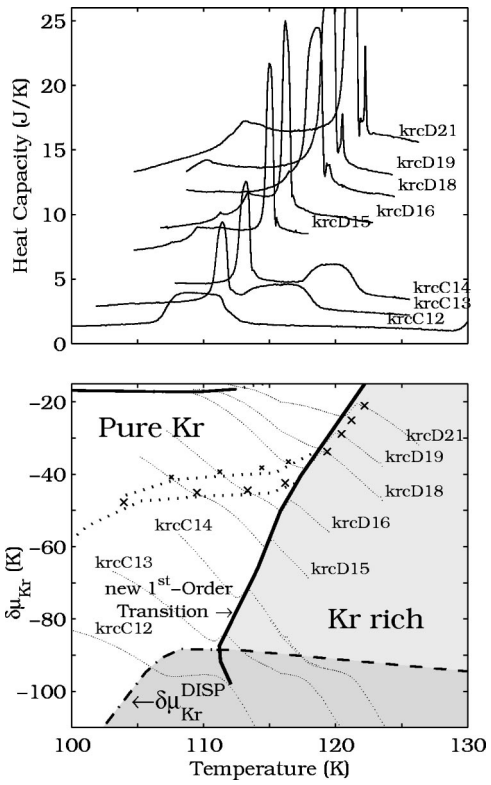

FIG. 10. Heat capacity and chemical potential data around a new coadsorption first-order phase boundary. Runs krcC12, 13, and 14 have normalized coverages of 2.05, 2.62, and 3.12 $\sqrt{3}\times\sqrt{3}$ monolayers, and runs krcD 15, 16, 18, 19, and 21 have nominal coverages of roughly 3.3, 3.8, 4.4, 5.5, and 6.8 ML.

95 K feature has been associated, for Kr on bare graphite, with the second layer triple point, and the 98 K feature appears on passing near the critical point of second layer condensation. As the coverage is increased (see run krcA09), above the critical density, the signal associated with the critical point disappears, while the 95 K melting signal remains as the second layer is completed. After completion of the second layer, the melting peak moves to higher temperatures with increasing coverage (runs krcA13-17), as is seen in the pure Kr data. Even a tiny peak found just below the main second layer melting peak, likely indicative of a second layer commensurability transition,[15], is reproduced just above the noise in the coadsorption data (at 107 K in krcA17, for instance). Another peak as seen at 95 K in krcA16 and 17, and, as seen in Fig. 9, this closely resembles a peak in the single species Kr data, which has been linked to the melting of the third layer of film.

The phase boundaries traced out by these coadsorption features closely overlap the pure Kr phase diagram in Fig. 8. Discrete locations in $(T,\delta\mu_{\mathrm{Kr}})$ at which the coadsorption heat capacity maxima occur are marked "×" (the tiny feature preceding second layer melting is marked with a small "×"). Also marked (○) are select points along the second and third first-order layering transitions, determined by points at which the coadsorption isotherm data display vertical steps, or, as viewed in the phase diagram plot in Fig. 8, where the experimental trajectories for different coverages converge to overlap in $(T,\delta\mu_{\mathrm{Kr}})$. These coadsorption data are plotted against the backdrop of the pure Kr phase boundaries, plotted as solid (first-order layering and reentrant layering transitions) and dotted lines (layer melting and commensurability transitions). Note the close overlap of the coadsorption and single species phase boundaries. The level of systematic disagreement between the phase boundaries in the pure Kr and coadsorption films, on the order of 1 K in $\delta\mu_{\mathrm{Kr}}$, is consistent with the error introduced by thermometry drift, at the level of 0.1 K in temperature, occurring between cooldowns, and, as such, cannot be associated with a true difference between the coadsorption and pure Kr systems.[36]

This overlap with the pure Kr phase diagram, in this region of $(T,\delta\mu_{\mathrm{Kr}})$, is consistent with the picture of a pure Kr film emerging in the coadsorption system. Additionally, the positions of the low temperature first-order layering transitions, in the second and third layers, and other details of the phase diagram (such as the commensurability transition in the second layer) will be sensitive to the underlying substrate potential. As such, the most reasonable explanation is that the Kr film is indeed adsorbing on the bare graphite substrate, as assumed in the previously discussed thermodynamic model of displacement.[12] Additionally, this confirms and extends to higher temperatures the findings of Abdelmoula, *et al.*[1], who observed x-ray diffraction patterns characteristic of the pure Kr monolayer on bare graphite after displacement of CCl_4 at 80 K. Finally, while the coadsorption system apparently evolves into a pure Kr multilayer at least at these relatively low temperatures, the large peak that is observed to emerge at higher temperatures (near 111 K in krcA09 in Fig. 8) has no analog in the pure Kr system. The new phase boundary associated with this peak is the subject of the next subsection.

C. A new first-order coadsorption phase transition

The calorimetry data in Fig. 10 show the onset of a new heat capacity feature, emerging from the high temperature side of the broad desorption feature (in krcC12) and then growing larger and sharper with increasing Kr coverage (runs krcC13 at 112 K and in subsequent runs). The phase boundary associated with this peak thus begins just below the completion of displacement around 112 K. Seen most clearly in the cooldown A heat capacity data of Fig. 8 and in the boundary traced out in the phase diagram, the peak moves with increasing coverage to slightly lower temperatures before turning, at roughly 111 K, toward higher temperature with increasing $\delta\mu_{\mathrm{Kr}}$. The broad desorption feature, discussed in Sec. IV A, is observed to move to temperatures above that of the new sharp peak (runs krcC13 and 14), tracing out a phase boundary, dashed $(--)$ in Fig. 10, that is nearly horizontal in $(T,\delta\mu_{\mathrm{Kr}})$. We associate the sharp heat capacity peak, unique to the coadsorption system, with a first-order phase boundary, plotted with a bold solid line in Fig. 10, that coincides with the completion of displacement at higher temperatures.

The chemical potential experimental trajectories in Fig. 10 experience a sharp ''glitch'' upon crossing the phase boundary defined by the heat capacity peaks, moving nearly parallel to the phase boundary before reapproaching the original trajectory. The temperature extent of this experimental trajectory ''glitch'' roughly coincides with the width of the heat capacity peak. This is characteristic of a system undergoing a first-order phase transition and is analogous to bulk melting at constant number and volume, where the system moves along the phase boundary as melting occurs, preserving the overall system density during the conversion between solid and liquid phases of different densities. While these films need not preserve the number of either species in the film (Kr can desorb into the gas phase and CCl_4 can enter bulk solid form), a discontinuity in the film density of either species as the phase boundary is crossed will result in the system following the phase boundary, adsorbing or desorbing atoms until the density is appropriate to move completely into the new phase.

The trajectories here shift toward higher chemical potentials along the phase boundaries as T is increased $[(d/dT)\delta\mu_{\mathrm{Kr}}>0]$. This positive shift in $\delta\mu_{\mathrm{Kr}}$ corresponds to increasing the Kr gas pressure, which comes from desorbing Kr from the film, and so the system is moving into a high temperature phase of lower density than the low T phase. Referring back to Fig. 6, a desorption feature does indeed accompany the heat capacity peak in run krcC13 near 112 K. The desorption contribution does not nearly account for the full peak size, indicating a true structural change in the film which increases entropy upon crossing into the high T phase. One also finds in this run, centered near 116 K, the broad desorption heat capacity peak, which is quantitatively explained almost entirely by the desorption contribution.

A given experimental trajectory does not move exactly parallel to the curve of heat capacity maxima, but rather moves along and through a narrow (roughly 1/2 K) zone, indicating a finite broadening of the phase boundary. We can, however, extrapolate coverage data for a given run on either side of the peak up to the phase boundary defined by the heat capacity maxima and determine that Kr density in the low temperature phase is denser than that in the high temperature phase by as much as 10% along the high coverage portions of the phase boundary. At the low coverage end, the density discontinuity vanishes, along with the heat capacity peak itself, into the mixed CCl_4/Kr phase.

The isotherm data, for 111.7 and 115.7 K, plotted in Fig. 4 suggest that we associate this new first-order phase boundary with the completion of displacement above 111 K. Here, the first-order phase boundary coincides, in $(T,\delta\mu_{\mathrm{Kr}})$ with the convergence of the coadsorption and pure Kr isotherm curves, where the coadsorbed Kr film density approaches that of a pure Kr film. The phase diagram accompanying the isotherm data in Fig. 4 indicates both the new first-order (FO) transition boundary and that associated with the onset of the broad desorption (DES) feature. Likewise, the chemical potentials at which these phase boundaries intersect the chosen isotherm temperatures are marked in the 111.7 and 115.7 K isotherm plots. The coadsorption isotherms at both temperatures exhibit a steep increase in adsorption leading up to the des boundary, but in both cases, at these higher temperatures, the Kr film density is still measurably less than that of the single species pure Kr film; the region just above this des feature is thus labeled the ''Kr rich'' mixture phase, in light gray in Figs. 1 and 10. At 111.7 K, the coadsorbed Kr density very nearly joins the pure Kr data when the first-order phase boundary is encountered (which is also very near to the onset of the desorption feature). At 115.7 K, where there is a larger separation in chemical potential between the FO and des features, the isotherm data also show a small jump in coadsorbed Kr in the vicinity of the FO boundary, bringing the coadsorbed Kr density very close to that of the pure Kr film density.

At these higher temperatures, where displacement of CCl_4 continues well into the second layer of Kr film growth, the overlap between the coadsorption and pure Kr isotherm curves is not as complete as at lower temperatures, with the Kr coadsorption coverage remaining several percent below that of the pure Kr system. It should be noted here that included in the ''film densities'' measured with our volumetric technique is a contribution from capillary condensate (volumetry just measures the number of Kr atoms condensed out of the gas phase), which becomes significant at higher coverages. As such, even if displacement of CCl_4 from the film is 100% complete, we might observe a slightly reduced density in the coadsorption system if, as expected, the ''overfilled'' CCl_4 monolayer inhibits Kr capillary condensate. As such, this final near approach to the pure Kr isotherm coinciding with the large heat capacity peak is a likely indication that this new first-order phase boundary is associated with the completion of displacement at temperatures above 112 K. Summarizing, while most of the displacement of CCl_4 occurs below the boundary marked ''des'' in Fig. 4, the coadsorbed Kr density remains measurably less than that of the pure Kr density until the first-order phase boundary is crossed. In this sense, the ''completion of displacement'' could be the final

purification of an already Kr rich film, in moving to the lower *T*, higher $\delta\mu_{Kr}$, side of the first-order phase boundary.

There is another reason to associate the first-order phase boundary with the completion of displacement. All the data on the low temperature side of the phase transition indicate a film of pure Kr on bare graphite. The phase boundaries for the second layer commensurability and melting transitions, shown in Figs. 3 and 10, overlap the pure Kr data until they ''collide'' with the first-order phase boundary. This is seen in the calorimetry data as the second layer melting peak merging into the large heat capacity feature, occurring between runs krcD16 and 18 in Fig. 10. At least from the observed phase transitions, the film acts like pure Kr on the low temperature side of the new first-order transition.

The fate of the second layer melting and commensurability transitions on encountering the first-order phase boundary is a probe of the nature of the high temperature phase labeled ''Kr rich.'' The second layer features are both clear, in Fig. 10, on the low-temperature side of the large peak in runs krcD15 and 16. In subsequent runs, these features ''disappear'' into the large peak. However, in runs krcD18 and higher, there is the clear emergence of another peak on the high-temperature side of the large heat capacity peak. We sometimes observe slight ''bounces'' in the heat capacity data immediately following a large peak, an artifact of the imperfect temperature control during an abrupt heat capacity change (the small feature just following the large peak in krcD15 is a possible example of this). However, the sharp peak that moves to higher temperatures in runs krcD18 and higher is not an artifact but a real heat capacity peak, as the temperature control and resulting heat capacity data have had sufficient time to recover from the initial peak. Seen in the phase diagram in Fig. 10, this sharp peak traces out a phase boundary similar to that of either the second layer melting or commensurability transition on the low temperature side of the dominant first-order transition, but the peak is much higher and sharper than those occurring in the pure Kr second layer. These data, unfortunately, cannot be extended to higher coverage and temperature, because they reach the high pressure limit of our apparatus (1000 Torr), so we cannot know if, for instance, there is a second transition involved, as there is for the second layer melting on the low temperature side of the new first-order phase boundary. We can only say that there is a phase transition occurring above the first-order phase boundary that is roughly in position to ''connect'' to the second layer pure Kr melting transition, but with a larger and sharper heat capacity signature.

The nature of the ''Kr rich'' phase occurring at high temperatures and relatively large Kr coverages remains unknown, other than that its density is slightly less than that of pure Kr, suggesting the presence of a CCl_4 ''contamination'' of the film. One possibility is that the newly observed first-order transition represents melting of the pure Kr monolayer into a mixed liquid film. The reduction in the melting temperature would be caused by the ''entropy of mixing'' introduced by the presence of CCl_4 in the liquid phase. This would also be consistent with the idea that this phase boundary represents the final displacement of CCl_4, as the Kr film would become pure upon crossing to the low *T*, high $\delta\mu_{Kr}$ side. However, unlike the large, first-order signal observed here in the coadsorption system, the monolayer melting heat capacity signal in the pure Kr film broadens and nearly disappears for densities well above the monolayer completion.[29,32] Additionally, pure Kr monolayer melting occurs at temperatures at least 15 K warmer than the first-order coadsorption transition discussed here (unfortunately the corresponding high vapor pressures involved at these higher temperatures do not permit us to pursue the pure Kr monolayer melting to higher coverages in our apparatus). This does not rule out the idea that the first-order transition here is connected with monolayer melting, but makes it difficult to perform a thermodynamic analysis of the transition as a ''perturbed'' version of pure Kr monolayer melting. Finally, if the just discussed sharp feature observed inside this ''Kr rich'' phase is indeed related to the second layer melting, it would suggest that the big first-order phase transition is not so catastrophic to the film as to disorder the second layer of Kr along with it, as might be expected for first layer melting.

Another possibility, given that the first-order phase boundary is not observed in the pure Kr system, is that the transition occurs in Kr that is adsorbed on top of the CCl_4 bulk. As already stated, the CCl_4 bulk occupies a substantial fraction of the surface area, and Kr adsorption atop the CCl_4 must occur at some level, perhaps more so at the higher temperatures where Kr liquid films might form. Several observations, however, suggest that the transition occurs in the Kr film adsorbed on graphite. First, there is the suggestive coincidence of the first-order phase boundary with the joining of the Kr density in the coadsorption system to that of the pure Kr film on bare graphite. Additionally, close overlap of the ''post-displacement'' coadsorption and pure Kr isotherm data, across the entire temperature range, suggests that significant Kr adsorption occurs only on the graphite surface liberated in the displacement process. If significant Kr adsorption on top of the bulk CCl_4 were to occur at temperatures approaching the 116 K bulk Kr triple point, as might be expected for a liquid film, there would be an excess of Kr in the 112 and 116 K scaled coadsorption isotherm data in Fig. 4, which is not found. Finally, in a rough comparison of the heat capacity data for runs crossing the first-order phase boundary in the B and C cooldowns, we find that the integrated peak energy or latent heat of the transition grows with increasing area of the film area of coadsorption (that is, with F^{-1}) rather than with the remaining area covered with excess CCl_4 [with $(1-F^{-1})$]. These indications all suggest that the phase boundary is associated with a first-order transition in the Kr film that displaces CCl_4 from the graphite surface. Structural measurements would complement this thermodynamic study in helping to understand this first-order phase transition.

D. High Kr coverages: Extension of the pure Kr phase diagram

Another original goal of this study was to extend to thicker films our earlier study of pure Kr films, which had revealed interesting reentrant layering and layer melting phenomena. Youn, Meng, and Hess first observed the reentrant

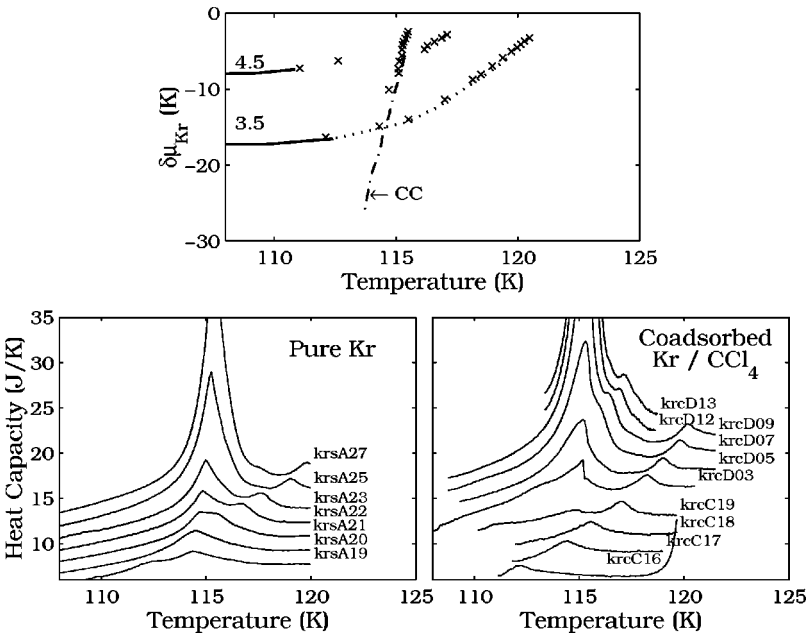

FIG. 11. (Top) Phase boundary crossings for coadsorbed Kr/CCl_4 (marked ×), plotted against the phase boundaries measured for pure Kr (solid, dotted, and "-··-" lines), extend the "3.5" and "4.5" phase boundaries for multilayer Kr. (Bottom) Heat capacity scans for Kr on bare graphite (left) and for the coadsorbed film (right) on the C and D cooldowns, with 430 and 600 stpcc CCl_4, respectively. Pure Kr data are from Day *et al.* (Refs. 15,16).

first-order layering transitions in Kr films between roughly 100 and 110 K in ellipsometry measurements.[20] The calorimetry data of Day *et al.* showed that the "3.5" transition, the first-order reentrant layering transition between roughly 2.5 and 3.5 layer coverages, extends, at the high temperature end, into a continuous phase boundary.[15,16] Not visible in the ellipsometry measurements, because there is no associated film density discontinuity, the phase boundary was detected as a line of heat capacity maxima in the calorimetry data, which, plotted in $(T,\delta\mu_{\mathrm{Kr}})$, ties into the endpoint of the first-order reentrant layering transition. However, calorimetry data for the "4.5" transition were completely obscured by the melting peak for capillary condensate near the 116 K bulk triple point. Growth and melting of Kr capillary condensate prevented study of the fourth and higher layers. Oversaturating a preadsorbed CCl_4 monolayer can, potentially, fill enough of the Grafoam substrate's small pores to delay the onset of Kr capillary condensate to higher chemical potentials and thus allow the study of thicker Kr films. As discussed in Sec. IV B, it appears that a pure Kr multilayer film forms after displacement, and thus the Kr / CCl_4 system could permit extension of the pure Kr multilayer phase diagram to thicker films.

Figure 11 shows heat capacity data for both pure Kr and coadsorbed Kr/CCl_4 for Kr coverages of three or more layers and in the vicinity of the bulk Kr triple point. For the pure Kr film data,[15,16] a central heat capacity peak appears below 115 K and, with increasing coverage grows and approaches the triple point near 116 K. This peak has been associated with the melting of unsaturated capillary condensate,[19] tracing a phase boundary (labeled CC in the phase diagram in Fig. 11) that closely follows the relation

$$\delta\mu=\left(\frac{Lv_s}{v_l-v_s}\right)\frac{T-T_t}{T}, \tag{5}$$

where T_t is the bulk melting point, L is the bulk latent heat of melting, and v_s and v_l are the solid and liquid specific volumes. Just below (near 112.5 K in krsA19) and above (near 116 K in krsA21 and moving to higher temperatures with higher coverage) this capillary condensate melting peak, there is another series of heat capacity features. The locations in $(T,\delta\mu_{\mathrm{Kr}})$ of these small heat capacity features link together to form a phase boundary which intersects the capillary condensate melting line and appears to connect to the reentrant layering "3.5" transition.

In the coadsorption data, we also see the series of peaks associated with the extension of the "3.5" transition, clearly moving from 112 K (krcC16) to 120 K (krcD09). Unlike the pure Kr data, the "3.5" peak never disappears into a capillary condensate feature. A capillary condensate peak is observed in the coadsorption system, but not until considerably higher coverages, at which the "3.5" transition has already passed to higher temperatures (the CC peak is clearly visible in krcD03, where we observe the "3.5" transition in excess of 118 K). The onset of Kr capillary condensate is thus suc-

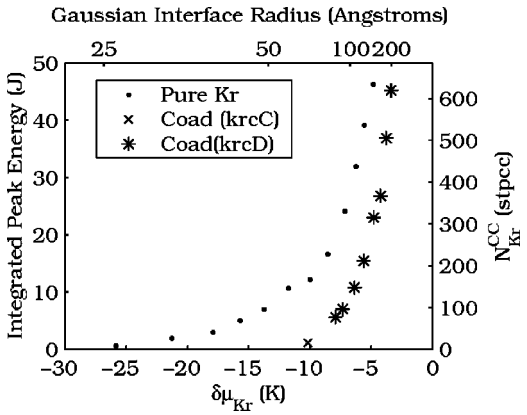

FIG. 12. Integrated capillary condensate peak energy as a function of chemical potential for single species Kr and for two coadsorption datasets (krcC and D). Pore radius, as calculated from Eq. (7), is shown at top, and the number of Kr atoms involved in capillary condensate melting, estimated using Eq. (6), is shown at right.

cessfully delayed to higher coverages in the coadsorption system, allowing clearer measurement of the film phase transitions at higher coverage. As both the ''3.5'' and CC transitions (marked $\times$ in the phase boundary shown in Fig. 11) overlap the phase boundary lines for the pure Kr system, the coadsorption technique indeed appears to permit relevant measurement of thicker Kr films.

The degree to which capillary condensate is suppressed in the coadsorption system is quantified in Fig. 12. The integrated energy of the capillary condensate melting peak E_{CC} measured for a run of a given Kr coverage or at a given chemical potential, gives an estimate of the number of Kr atoms N_{Kr}^{CC}, involved in capillary condensate[39]

$$E_{CC} \equiv \int C_{peak} dT = N_{Kr}^{CC} L. \tag{6}$$

Likewise, the measured chemical potential indicates the capillary condensate interface Gaussian radius of curvature D as given by the Kelvin Equation,[38]

$$\delta\mu^{CC} = -\frac{v\sigma}{D}, \tag{7}$$

where σ and v are the surface tension and specific volume of the relevant bulk phase. Plotting the peak energy as a function of chemical potential thus indicates, for the pure Kr system, the volume in the Grafoam substrate accessible for capillary condensate in pores up to a given interface radius, and, for the coadsorption system, how effective CCl_4 is in filling those pores and preventing Kr capillary condensate.

Figure 12 indicates that capillary condensate becomes significant for pore radii on the order of 25 Å for pure Kr, but not until radii of roughly 75 Å, corresponding to $\delta\mu_{Kr} \approx -10$ K, in the coadsorption system on cooldowns C and D. At $\delta\mu_{Kr} \approx -15$ K, where the ''3.5'' phase boundary crosses the capillary condensate melting curve, the pure Kr system has roughly half a monolayer condensed in capillary condensate, nearly 100 stpcc, whereas the coadsorption system shows basically none, thus allowing measurement of the ''3.5'' phase boundary without the interference of capillary condensate. As such, the smallest pores are very effectively filled by the CCl_4. Earlier cooldowns did not show as much success in inhibiting capillary condensate, likely because the cooldowns were not well enough controlled to allow the preadsorbed CCl_4 to find and equilibrate into the smallest pores of the system. Referring to the D cooldown data at high chemical potentials in Fig. 12, the integrated heat capacity data indicate that there are as many as 300 fewer stpcc of melting Kr capillary condensate than in the pure Kr data. Given a factor of roughly three in the ratio of the bulk condensed volumes of the two species, this means that approximately 100 stpcc of CCl_4 occupies the pores in the place of Kr. This is a relatively small fraction of the 600 stpcc dose of CCl_4 that was used in the D cooldown, indicating that not all the CCl_4 entered the pores in equilibrium fashion even in the most controlled cooldown, consistent with excess CCl_4 occupying a good portion of the graphite surface.

While the suppression of Kr capillary condensate shown in Fig. 12 is not as great as expected for the large dose of CCl_4 used, it does allow us to reach higher Kr chemical potentials than with pure Kr, reaching $\delta\mu_{Kr} \approx -5$ K. This is just sufficient to permit the first observation of what is likely an extension of the ''4.5'' reentrant layering transition. We observe this as a small but clear peak poking up as a ''right shoulder'' on the capillary condensate peak seen in krcD07 and subsequent runs in Fig. 11. There is a logical connection between these peaks above the capillary condensate peak and the very small, broad features seen at slightly lower temperatures in lower coverage runs (111 K in krcC19 and 113 K in krcD03). The positions in $(T, \delta\mu_{Kr})$ of these features (see phase diagram in Fig. 11) make it likely that they can be linked together as a continuous phase boundary extension to the ''4.5'' first-order reentrant layering transition, with the heat capacity signal obscured between 113 and 116 K by the encroaching signal from capillary condensate melting. The slight sharpening of the heat capacity feature at higher temperatures is likely related to the upturn in chemical potential of the phase boundary and thus the more ''direct'' crossing of the phase boundary by experimental trajectories.

Note that the heat capacity peaks associated with the extension of the ''3.5'' and ''4.5'' transitions have been followed here to at least 8 and 6 K, respectively, beyond the first-order reentrant layering endpoints visible in the data of Hess *et al.*[20] without diminishing in size. As such, it is likely that these features are not associated with the system passing near to reentrant layering critical endpoints, but rather represent the crossing of a continuous phase boundary that connect to the first-order reentrant layering boundaries.

V. CONCLUDING REMARKS

A. Nature of coadsorption experiments and displacement

The calorimetric evidence that displacement of CCl_4 by Kr at low temperatures results in a pure Kr film adsorbed on bare graphite is consistent with the results of the 80 K x-ray diffraction study by Abdelmoula *et al.*[1] Our study extends this observation to much higher temperatures, with the coadsorption phase diagram overlapping that of pure Kr on graphite in the multilayer regime to temperatures in excess of the 116 K bulk Kr triple point. Additionally, this pure film of Kr is observed to occur by a continuous displacement process. This is most clear at higher temperatures, where we see continuous evolution from a pure CCl_4 film into a Kr rich mixed film of two or even three layers, before finally experiencing a slight density discontinuity on crossing a newly observed first-order phase boundary into a pure Kr film. The continuous nature of the CCl_4 displacement was first observed in the volumetric isotherm data[12] and implies the existence of a mixed Kr/CCl_4 film. This is confirmed in the calorimetric study, with a clear heat capacity signal arising from the desorption of Kr as displacement is continuously reversed with increasing temperature, presumably accompanied by the reaquisition of the graphite surface by CCl_4, which enters into a solution film with Kr. The existence of mixed films preceding the completion of displacement was also found at intermediate temperatures in x-ray diffraction studies of the Kr/SF_6 system.[9]

Aspects of both equilibrium and nonequilibrium physics are observed in the Kr/CCl_4 coadsorption experiments described here. The excess and displaced CCl_4 does not all wind up frozen into the pores of the graphite as one might expect from equilibrium arguments, but rather continues to occupy a substantial fraction of the graphite surface even after film density and phase boundary measurements indicate formation of a pure Kr film on bare graphite. This shared surface is inconsistent with equilibrium phase rule arguments.

On the other hand, the measurements here show CCl_4 reversibly being displaced from, and then readsorbing onto, the graphite substrate on experimental time scales. Additionally, the measured coadsorption phase boundaries and equation of state data for the Kr density in the coadsorbed film are reproduced between cooldowns employing different amounts of adsorbed CCl_4 and with different amounts of surface occupied by the remaining CCl_4. This, and the observation that CCl_4 displacement by both Kr and CH_4 results in the same calculated CCl_4 saturated spreading pressure $\phi^0_{CCl_4}(T)$ over a wide temperature range, suggests that the CCl_4 chemical potential remains fixed in these displacement experiments, a function of temperature that is independent of the ''excess'' amount of CCl_4, the type of inert gas adsorbate, and the inert gas vapor pressure. This is consistent with the simple model of displacement we have previously presented.[12] However, how close this chemical potential is to the true equilibrium bulk potential value $\mu^0_{CCl_4}(T)$ where equilibrium thermodynamics says displacement should occur, can not be determined from these measurements.

In light of both the slow kinetics and the observed unwillingness of the CCl_4 to leave the graphite surface completely in order to form macroscopic crystals, the existence of a metastable crystalline phase in the excess and displaced CCl_4 is likely. Without speculating on the nature of these crystals, we note that the crystal phase diagram observed for bulk CCl_4 grown in contact with graphite at higher temperatures does not correspond exactly with that of bulk CCl_4 grown in the absence of graphite.[10,11] Specifically, on graphite there is a tendency to stabilize to slightly lower temperatures the high temperature rhombohedral phase, which, unlike the equilibrium low-temperature monoclinic crystalline phase, has crystal planes with an equilaterally symmetric ''$\sqrt{3} \times \sqrt{3}$'' structure characteristic of the 2D low-temperature solid formed on graphite. It is not known whether such a metastable crystalline structure, nucleated at the graphite surface, is the actual ''bulk'' phase relevant to low temperature displacement of CCl_4.

B. Coadsorption and the study of thicker pure Kr films

The apparently pure film of Kr formed in the coadsorption system and the successful occupation of the exfoliated graphite substrate's small pores with excess CCl_4 allows a slight extension of the multilayer Kr phase diagram. Like the reentrant layering transition between coverage of roughly 2.5 and 3.5 layers, that associated with 3.5–4.5 also appears to extend to higher temperatures, beyond the bulk triple point, as a continuous transition [the first-order density discontinuity associated with the 3.5–4.5 reentrant layering transition ends around 110 K (Ref. 20).]

The presence of these apparently continuous extensions of the reentrant layering transitions is relevant to recent theoretical studies linking preroughening and top layer melting.[23,24] In the simulation work of Celestini *et al.*, solidification of the surface layer is found to be accompanied by a discontinuous population, to half occupancy, of the next layer. One might expect melting in the top film layer to occur also at temperatures beyond the endpoint of the first-order, half-integral layering transition. Consistent with this scenario, it is possible that the extension transitions observed here are extensions of the top layer melting transition above the endpoint of the reentrant layering density discontinuity, where film growth is fully continuous. A ''zippering'' connection between the integral first-order low temperature layering transition and the low temperature end of the reentrant half-coverage phase transitions has already been demonstrated, both experimentally and theoretically[15,21]. As such, for at least the third and fourth layers (referring back to the phase diagram in Fig. 1), there is a possible scenario of single melting phase boundaries connecting at low temperatures to the first-order (integral) layering transitions, coinciding (or nearly coinciding) at intermediate, ''prerough,'' temperatures with a first-order reentrant layering transition, and finally running to temperatures above the bulk triple point as continuous layer melting.

While useful in allowing a modest contribution to the multilayer Kr film phase diagram, the coadsorption technique is not likely to extend the study to much thicker films. As is clear from Fig. 12, the volume accessible to Kr capillary condensate greatly increases as one reaches chemical potentials close enough to bulk saturation to form films of five or more layers, demanding larger amounts of preadsorbed CCl_4 to prevent Kr capillary condensate. With the increasing amounts of CCl_4 adsorbed, less surface area is available for the displacing film of Kr; already, in cooldowns C and D, the scale factor, F, is greater than 2, indicating that less than half the total substrate is available for film growth. As the area available for adsorption decreases, the already small heat capacity signals arising from phase transitions in the upper film layers diminish.

C. New first-order transition unique to coadsorption

Perhaps the most interesting discovery of this calorimetry study is the observation of a new first-order phase transition unique to Kr/CCl_4 coadsorption. The large heat capacity signal is accompanied by clear evidence, from the chemical potential data, of the system following the phase boundary during the transition, and coincides with the Kr density becoming, on the low T side, approximately equal to that of a pure Kr film at the same point in $(T, \delta\mu_{Kr})$. While the film behaves like pure Kr on the low temperature side of the phase transition, linking the transition with the completion of displacement, the high temperature phase is not known, except that its Kr density is slightly less than that of a pure Kr film and that it is formed in a continuous (and thus single phase) displacement process beginning with a solid CCl_4 monolayer. It is most simple to link the first-order transition

to melting of a pure Kr monolayer into a mixed liquid phase, but this interpretation is complicated by the apparent penetration of second layer melting across the first-order phase boundary, which would imply the unlikely existence of a solid second layer of Kr atop a mixed liquid phase. At these higher temperatures where the first-order phase transition is observed in our thermodynamic measurements, a structural study, analogous to that performed for Kr/SF_6 by Castro and Thomas,[9] could be instrumental in determining the nature of this phase transition and in understanding the continuous evolution of a Kr rich mixed phase from a pure CCl_4 monolayer film.

*Current address: Dipartimento di Fisica, Università di Trento, Via Sommarive 14, 38050 Povo (TN), Italy

[1] M. Abdelmoula, T. Ceva, B. Croset, and N. Dupont-Pavlovsky, Surf. Sci. **272**, 167 (1992).
[2] H. Asada, S. Doi, and H. Kawano, Surf. Sci. Lett. **273**, 403 (1992).
[3] M. Bouchdoug, J. Menaucourt, and A. Thomy, J. Phys. (France) **47**, 1797 (1986).
[4] A. Razafitianamaharavo, N. Dupont-Pavlovsky, and A. Thomy, J. Phys. (France) **51**, 91 (1990).
[5] A. Razafitianamaharavo, P. Convert, J.P. Coulomb, B. Croset, and N. Dupont-Pavlovsky, J. Phys. (France) **51**, 1961 (1990).
[6] J. Menaucourt and C. Bockel, J. Phys. (France) **51**, 1987 (1990).
[7] N. Dupont-Pavlovsky, M. Abdelmoula, S. Rakotozafy, J.P. Coulomb, B. Croset, and E. Ressouche, Surf. Sci. **317**, 388 (1994).
[8] H. Asada, H. Seiyama, and M. Takechi, Adsorpt. Sci. Technol. **15**, 271 (1997).
[9] M.A. Castro and R.K. Thomas, Surf. Sci. **399**, 212 (1998).
[10] P.W. Stephens and M.F. Huth, Phys. Rev. B **32**, 1661 (1985).
[11] M. Abdelmoula, T. Ceva, B. Croset, and N. Dupont-Pavlovsky, Surf. Sci. **274**, 129 (1992).
[12] W.J. Weber and D.L. Goodstein, Phys. Rev. Lett. **83**, 3888 (1999).
[13] Coexistence of two distinct film phases implies exact coincidence of the spreading pressures $\phi(T,\mu_{CCl_4},\mu_{Kr})$ for the two phases. For these two spreading pressure surfaces to exactly coincide over a finite range of μ_{Kr}, at fixed T and for $\mu_{CCl_4}=\mu^0_{CCl_4}(T)$, is extremely unlikely. A more detailed discussion of the thermodynamics relevant to coadsorption and displacement is given in Ref. 29.
[14] F. Hommeril and B. Mutaftschiev, Phys. Rev. B **40**, 296 (1989).
[15] P. Day, M. LaMadrid, M. Lysek, and D. Goodstein, Phys. Rev. B **47**, 7501 (1993).
[16] P.K. Day, Ph.D. thesis, California Institute of Technology, 1993.
[17] M.J. Lysek, M.A. LaMadrid, P.K. Day, and D.L. Goodstein, Phys. Rev. B **47**, 7389 (1993).
[18] P. Day, M. Lysek, M. LaMadrid, and D. Goodstein, Phys. Rev. B **47**, 10 716 (1993).
[19] M. Lysek, M. LaMadrid, P. Day, and D. Goodstein, Langmuir **9**, 1040 (1993).
[20] H.S. Youn, X.F. Meng, and G.B. Hess, Phys. Rev. B **48**, 14 556 (1993).
[21] P.B. Weichman, P. Day, and D. Goodstein, Phys. Rev. Lett. **74**, 418 (1995); P.B. Weichman and A. Prasad, *ibid.* **76**, 2322 (1996); A. Prasad and P.B. Weichman, Phys. Rev. B **57**, 4900 (1998).
[22] J.M. Phillips, Q.M. Zhang, and J.Z. Larese, Phys. Rev. Lett. **71**, 2971 (1993).
[23] F. Celestini, D. Passerone, F. Ercolessi, and E. Tosatti, Phys. Rev. Lett. **84**, 2203 (2000).
[24] E.A. Jagla, S. Prestipino, and E. Tosatti, Phys. Rev. Lett. **83**, 2753 (1999).
[25] G.D. Halsey, J. Chem. Phys. **16**, 931 (1948); T.L. Hill, *ibid.* **15**, 767 (1947); W. A. Steele, *The Interaction of Gases with Solid Surfaces* (Pergamon Press, Oxford, 1974).
[26] Courtesy of Union Carbide.
[27] M. J. Lysek, Ph.D. thesis, California Institute of Technology, 1992.
[28] M.J. Lysek, P. Day, M. LaMadrid, and D. Goodstein, Rev. Sci. Instrum. **63**, 5750 (1992).
[29] W. J. Weber, Ph.D. thesis, California Institute of Technology, 2000.
[30] This corresponds to a Langmuir model estimate, as developed in, for instance, L. W. Bruch, M. W. Cole, and E. Zaremba, *Physical Adsorption: Forces and Phenomena* (Clarendon Press, Oxford, 1997) and applied in Ref. 29.
[31] T. Takaishi and Y. Sensui, Trans. Faraday Soc. **59**, 2503 (1963).
[32] D.M. Butler, J.A. Litzinger, G.A. Stewart, and R.B. Griffiths, Phys. Rev. Lett. **42**, 1289 (1979).
[33] D.M. Butler, J.A. Litzinger, and G.A. Stewart, Phys. Rev. Lett. **44**, 466 (1980); E.D. Specht, A. Mak, C. Peters, M. Sutton, R.J. Birgenau, K.L. D'Aminco, D.E. Moncton, S.E. Naylor, and P.M. Horn, Z. Phys. B: Condens. Matter **69**, 347 (1987).
[34] A. Thomy and X. Duval, J. Phys. I **67**, 286 (1970); A. Thomy and X. Duval, *ibid.* **67**, 1101 (1970).
[35] The 112 and 116 K data have been extended to higher coverages, crossing the first-order phase transition, with data from the early ''krcA'' run. These data were not measured with isotherms in mind, and thus the films were not grown with same ''quasistatic,'' purely adsorption branch technique described in Sec. III. The data overlap the other coadsorption data well, scaled with $F=1.21$, however, and are shown here to highlight the slight jump in coverage observed near the first-order phase boundary.
[36] Remeasuring selected portions of the pure Kr dataset produced a similar slight ''movement'' in the apparent position of the phase boundaries. This was used to recalibrate the thermometry for the coadsorption data. However, slight variations in this thermometry calibration were observed to occur at every new cooldown of the system, and a relative temperature uncertainty on the order of 0.1 K is realistic for comparing data from the different datasets (see Ref. 29).
[37] Y. Nardon and Y. Larher, Surf. Sci. **42**, 299 (1974).
[38] R. Defay and I. Prigogine, *Surface Tension and Adsorption* (Wiley, New York, 1966).
[39] L has been shown to be different for small crystals Ref. 27, such as those capillary condensed in the pores of exfoliated graphite, but the bulk value of L, as estimated from the bulk saturated vapor pressure data, suffices for this rough estimate.